Materials and Structures, 1995, **28**, 210–219

Design and structural applications of stress–crack width relations in fibre reinforced concrete

HENRIK STANG[1], VICTOR C. LI[2], HERBERT KRENCHEL[1]

[1] *Department of Structural Engineering, Technical University of Denmark, Building* 118, *DK-2800 Lyngby, Denmark*

[2] *Department of Civil & Environmental Engineering, University of Michigan, Ann Arbor, MI 48109-2125, USA*

The stress–crack width relationship has been shown to be the key to an understanding of fracture propagation in and mechanical behaviour in tension of fibre reinforced concrete materials and structures. A model is derived for the stress–crack width relationship for randomly oriented short fibre composites which takes hybrid fibre systems and possible fibre rupture into account. It is shown how this stress–crack width relationship can be included in a structural model for the prediction of crack widths in reinforced concrete structures. With this combination of models a rational design tool for the design of composite materials and structures has been established. It is shown how different fibre systems can be tested for structural applicability and how combined material and structural optimization can take place.

1. INTRODUCTION

Extensive research into the mechanical properties of fibre reinforced concrete and other fibre reinforced cementitious materials has taken place for many years, especially since the pioneering work of Romualdi and Batson [1] on steel fibre reinforced concrete. Many promising results have been reported showing improved strength, strainability and ductility. An abundance of papers and proceedings on the subject can be found along with a fair number of text books, see, e.g., Bentur and Mindess [2] and Balaguru and Shah [3]. A number of standards have been established for testing as well as for the quality assurance of fibre reinforced concrete and other fibre reinforced cementitious materials.

However, looking into the application of fibre reinforced cementitious materials in general and fibre reinforced concrete in particular it is generally agreed that there is a discrepancy between the promising results from the research community and the not very widespread use of these composite materials.

One explanation for this discrepancy is that only a few structural design tools are available which can actually predict the mechanical behaviour of structures composed of fibre reinforced concrete. This is due to the fact that primarily the post-peak behaviour is affected by the presence of fibres, see, e.g., Stang [4], while most design tools used by the structural concrete designer take into account only pre-peak behaviour (typically Young's modulus and compressive strength).

Another explanation is that the addition of fibre reinforcement to the concrete mix adds so many design parameters (fibre substrate, fibre geometry expressed as diameter, length, and possible irregularities such as hooks and enlarged ends, fibre volume concentration, possibly also fibre orientation, and maybe even combinations of several fibre types) to the concrete structure which already is described by quite a large number of design parameters (concrete strength, stiffness, conventional reinforcement type, conventional reinforcement geometry and structural geometry) that a rational design approach appears to be an overwhelming task.

Even though, as mentioned above, the use of fibre reinforcement is not very widespread, a number of structures where the use of fibre reinforcement seems obvious, possibly in connection with traditional reinforcement, have been identified. Among these are structures with strict requirements on the crack widths [5]. Such structures are typically fatigue loaded concrete structures, watertight reinforced concrete structures or reinforced concrete structures in aggressive environments.

It is the purpose of the present paper to show how a rational design approach can be taken in the case of designing a concrete structure with a specific crack width requirement in the serviceability limit state using a combination of conventional reinforcement and fibre reinforcement.

In this approach the fibre reinforced concrete material is considered a composite material with specific material properties which can be predicted from the material composition using a model which is described in the following. This model can handle any number of fibre types and takes into account the fibre orientation, fibre geometry and fibre strength, and is an extension of a model proposed previously by Li, Stang and Krenchel [6]. The mechanical model for the prediction of crack widths in concrete structures with a combination of conventional reinforcement and fibre reinforcement is based on a structural model proposed by Stang and Aarre [5]. The original structural model takes only empirical data as input. Here it is shown how this model can also take the composite material model as input. This

0025-5432/95

combination of models makes it possible to make predictions on the structural level taking not only geometrical design parameters as input but also parameters describing the material composition, i.e., choice of fibre system.

Consequently, the benefit on the structural level from a modification on the material level can be predicted readily using the proposed models, and a rational optimization process is possible.

2. STRESS–CRACK WIDTH RELATIONSHIP

It is assumed that the fibre reinforced materials considered here are materials which show an essentially linear response in uniaxial tension up to peak load. After peak a discrete crack is formed. It is furthermore assumed that the discrete crack formation is dominated by the stress–crack width relationship. This is a well known approach in the description of crack formation in plain concrete, suggested originally by Hillerborg [7]. Later this approach was also suggested for use in the description of the formation of cracks in fibre reinforced concrete [5, 8, 9].

Since the fibre reinforcement has a substantial effect on the stress–crack width relationship but hardly any influence on the pre-peak behaviour, a micromechanical model is derived for the stress–crack width relationship. This model is able to predict the stress–crack width relationship for small crack widths (crack widths allowed in concrete structures are typically less than 0.3 mm) as a function of the stress–crack width relationship for the plain concrete without fibres and the type and amount of fibre reinforcement used.

The micromechanical model takes the model developed by Li, Stang and Krenchel [6] as a starting point. Essentially, this model describes the stress σ_c carried across a crack in the fibre reinforced concrete as a function of the crack width w in the following way:

$$\sigma_c(w) = \sigma_a(w) + \sigma_f(w) + \sigma_{ps}(w) \tag{1}$$

where $\sigma_a(w)$ is an empirical expression for plain concrete aggregate bridging controlled by two parameters w_0 and p which have to be determined empirically [6]:

$$\sigma_a(w) = \frac{\sigma_{mu}}{1 + \left(\frac{w}{w_0}\right)^p} \tag{2}$$

where σ_{mu} is stress in the plain concrete at first crack.

The term σ_f is the fibre bridging contribution. The concept behind this term is fibre debonding and subsequent pull-out against a frictional resistance τ and inclined fibres acting as flexible ropes passing over a frictional pulley described through the snubbing coefficient f. The original model was derived by Li [10] and developed further by Li, Stang and Krenchel in [6], resulting in an implicit type of relationship between σ_f and w:

$$\sigma_f = \sigma_f(\delta) \tag{3}$$

and

$$w(\delta) = \delta + \frac{4\alpha}{V_f E_f}\sigma_f(\delta) \tag{4}$$

where δ is the crack opening without the so-called Cook–Gordon effect or pre-debonding of fibres [6, 11]. The Cook–Gordon model suggests that fibre debonding from the matrix takes place ahead of the matrix crack, resulting in the formation of a pre-debonded zone adding to the compliance of the bridging fibres. The parameter α is the so-called Cook–Gordon parameter describing the length of the pre-debonded zone, V_f is the fibre volume concentration, E_f is Young's modulus of the fibres, while $\sigma_f(\delta)$ is the fibre bridging stress function. The fibre bridging stress function used in [6] takes into account the following micromechanical parameters: fibre length L_f, fibre diameter d_f, snubbing coefficient f, frictional resistance τ, fibre volume concentration V_f, Young's modulus of fibres E_f, and finally Young's modulus of plain concrete or matrix E_m.

In the fibre bridging stress function the following relationship between τ and δ is introduced in order to take into account (in an approximate way) slip-hardening or slip-weakening:

$$\begin{aligned} &\tau = \tau_0 && \text{for } \delta \le \delta^* \\ &\tau = \tau_0 + a_1\delta + a_2\delta^2 && \text{for } \delta > \delta^* \end{aligned} \tag{5}$$

where δ^* is the crack opening (without the Cook–Gordon effect) corresponding to complete debonding of all fibres and given by [6]:

$$\delta^* = \frac{\tau L_f^2(1 - V_f)E_m}{((1 - V_f)E_m + V_f E_f)E_f d_f} \tag{6}$$

Finally, the term σ_{ps} takes into account that the fibres are carrying load through elastic strain when the first crack is formed. As a first approximation the following relationship was used indicating a linear decay from the onset to complete pull-out:

$$\begin{aligned} &\sigma_{ps}(w) = \sigma_{ps}^0 \frac{w^* - w}{w^*} && \text{for } w \le w^* \\ &\sigma_{ps}(w) = 0 && \text{for } w > w^* \end{aligned} \tag{7}$$

with

$$\sigma_{ps}^0 = \left(1 - \frac{\varepsilon_{mu} E_f d_f}{4L_f\tau_0}\right)\varepsilon_{mu} E_f V_f \tag{8}$$

and

$$w^* = w(\delta^*) \tag{9}$$

(see Equation 4). In Equation 8 ε_{mu} denotes the strain in the plain concrete at the formation of the first crack, $\varepsilon_{mu} = \sigma_{mu}/E_m$.

It is shown in [6] that it is essential to include fibre pre-stressing as well as both the Cook–Gordon effect and the friction–slip relationships 5 and 6 in order to capture essential features in the stress–crack width relationships of fibre reinforced concrete. On the other hand when these effects are included it is shown in [6] that very good agreement with experimental findings can be

achieved, e.g., the effect on the stress–crack width relation from changing the fibre volume concentration can be predicted accurately.

However, fibre volume concentration is not the only important design parameter. Fibre length is equally important, and care should be taken in using the above relations to model the effect of fibre length since fibres are likely to fracture during the debonding process if their shortest embedded length is longer than the critical length and since fibre rupture is not included in the model derived by Li in [10]. This effect was included in a similar model derived by Maalej *et al.* [12]. The model is described in detail in [12] and will not be re-derived here. The rather lengthy expressions for $\sigma_f(\delta)$ can be found in Appendix A. In the present work these expressions for the fibre bridging stress have been used. These new expressions for σ_f are functions of the same micromechanical parameters as mentioned for the simpler expression above; however, now the tensile strength of the fibres σ_{fu} has been added to the list.

In order to optimize the fibre reinforced material it is also necessary to consider the use of hybrid systems which could be combinations of different fibre lengths of the same fibre type or combinations of different fibre types. This can be done by introducing fibre bridging terms in Equation 1 for each new combination of micromechanical parameters: length, diameter, stiffness, strength and bonding properties,

$$\sigma_c(w) = \sigma_a(w) + \sum_{I=1}^{F} \sigma_f^I(w) + \sum_{I=1}^{F} \sigma_{ps}^I(w) \qquad (10)$$

where F is the number of different fibre systems, and where the functions $\sigma_f^I(w)$ and $\sigma_{ps}^I(w)$ use the relevant micromechanical parameters: L_f^I, d_f^I, f^I, τ_0^I, a_1^I, a_2^I, α^I, V_f^I, E_f^I and finally σ_{fu}^I for the Ith fibre system.

Care should be taken during superposition of the second term since different δ for each fibre system should be used to ensure that the crack widths including the Cook–Gordon effect are the same:

$$\sigma_f^I = \sigma_f^I(\delta^I) \qquad (11)$$

and

$$w(\delta^I) = \delta^I + \frac{4\alpha^I}{V_f^I E_f^I} \sigma_f^I(\delta^I) \qquad (12)$$

This requirement implies the calculation of the total fibre bridging stress $\sum_{I=1}^{F} \sigma_f^I(w)$ due to all fibre types for a given crack opening w.

3. STRUCTURAL CRACK WIDTHS

The theoretical model for structural crack widths presented here was developed by Stang and Aarre [5] as a tool to be used in the prediction of crack widths in concrete structures where fibre reinforcement is used as crack controlling reinforcement in addition to conventional reinforcing bars which primarily have a load carrying function.

It is meant to be an equivalent of the type of semi-empirical formulae which are found in most codes for the use of structural concrete, e.g., in the Danish Code of Practice for the Structural Use of Concrete, DS-411 [13], where the crack width w is expressed as a function of stress in the reinforcing bars under service load and a geometrical parameter describing the size of the rebars and the effective reinforcing degree measured in a specified concrete area around the tensile reinforcement under consideration.

It is characteristic of this type of formula that it has quite a wide range of applicability since the only input parameters are the rebar stress and some geometrical quantity which can be defined for a wide range of structures.

On the other hand, it is impossible to extend the use of such formulae to non-traditional types of concrete, e.g., fibre reinforced concrete (FRC), and non-traditional types of rebar, e.g., non-steel rebar, because of the empirical nature of the formulae.

The model developed in [5] has the same type of geometrical generality, i.e., it is possible to apply the model to a wide range of structures by characterizing the structure using the effective reinforcing degree and the diameter of the reinforcing bars. On the other hand, much more detailed information regarding the mechanical properties of the concrete and the rebar is included in the model.

The model is described in detail in [5], and in the following the link between the stress–crack width model and the structural model will be described.

3.1 Material characterization

The fibre reinforced concrete is assumed to be linear elastic in tension up to the maximum stress σ_{frc}^u with Young's modulus E_{frc} and Poisson's ratio v_{frc}.

After the maximum stress and strain have been reached a discrete crack is formed in the material and this crack is characterized mechanically by the stress–crack width relationship $\sigma_{frc}^{crk}(w)$ where σ_{frc}^{crk} is the stress transferred over the discrete crack in the material, while w is the crack opening.

The reinforcing bars are assumed to be linear elastic. Thus, the mechanical properties are characterized through the elastic constants E_s and v_s, the Young's modulus and Poisson's ratio, respectively.

3.2 The geometrical model

A plane model of a prism consisting of a conventional reinforcing bar with thickness $2t$ surrounded by a layer of fibre reinforced material with thickness b is modelled as shown in Fig. 1. A total number N of cracks have been formed in the fibre reinforced material. The total length of the element is $2(N + 1)(l + d)$ corresponding to a spacing of $2(l + d)$ between discrete macrocracks in the fibre reinforced material. A coordinate system is placed as shown in the figure. It is assumed that there is

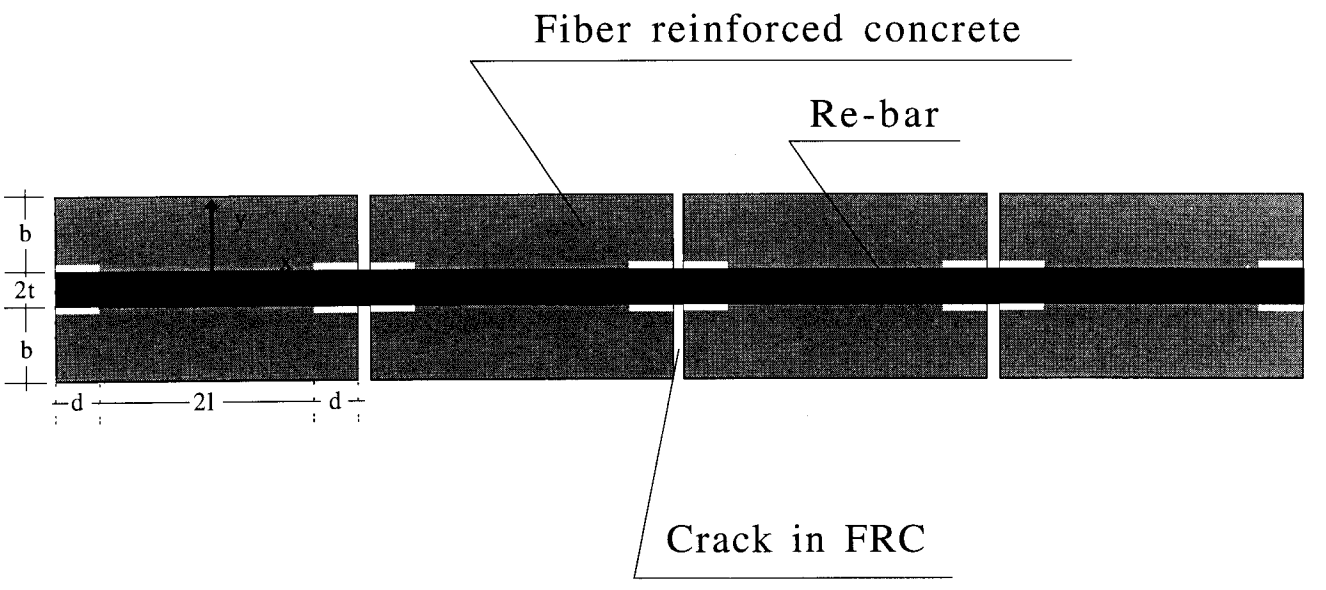

Fig. 1 The geometrical model used in the structural crack width model.

displacement continuity on the fibre reinforced concrete/reinforcing bar interface for $-l < x < l$ while the interface is stress free on the interface for $-(l+d) < x < -l$ and $l < x < l+d$, allowing for the modelling of debonding between the reinforcing bar and the fibre reinforced concrete (FRC).

A structural crack density parameter β_1 is introduced:

$$\beta_1 = \frac{t}{l+d} \tag{13}$$

Furthermore, the effective geometrical reinforcing degree is defined by:

$$\phi = \frac{t}{t+b} \tag{14}$$

The fibre reinforced material is assumed to be linear elastic between the cracks while the stress–crack width relation is the constitutive relation governing the opening of the cracks.

3.3 Calculation procedure

A complete (implicit) analytical solution is derived for the model described above and described in detail in [5]. Analytical solutions, as functions of overall strain, are presented for mean crack width, maximum stress in the FRC material, maximum stress in the rebar, and stress carried across the cracks in the FRC material.

The calculation of crack widths under different external loadings is now performed according to the following algorithm.

The starting point for the calculation is zero overall strain and a (large) distance between the discrete cracks. The strain is now increased in small steps. For each step the complete solution is determined using a simple bisection iteration scheme to solve the nonlinear equations which form the total solution. The maximum stress in the FRC material is calculated and it is checked whether the maximum stress in the FRC material $\sigma_{\text{frc}}^{\max}$ exceeds the ultimate tensile strength $\sigma_{\text{frc}}^{\text{u}}$.

When the ultimate tensile strength of the FRC material is exceeded, the distance between cracks is adjusted so that $\sigma_{\text{frc}}^{\max} = \sigma_{\text{frc}}^{\text{u}}$ corresponding to the formation of new discrete cracks.

The result of the calculation is corresponding values of overall strain, maximum stress in the reinforcing bar (at the discrete cracks in the FRC material), stress in the FRC material at the cracks, crack opening, and crack spacing.

3.4 Connection to the stress–crack width model

The structural crack width model is connected to the stress–crack width model and the micromechanical parameters in the following way. According to standard elastic analysis, see, e.g., Krenchel [14], the Young's modulus for the fibre reinforced concrete is calculated according to:

$$E_{\text{frc}} = \left(1 - \sum_{I=1}^{F} V_{\text{f}}^{I}\right) E_{\text{m}} + \sum_{I=1}^{F} \eta_{\text{l}}^{I} \eta_{\theta}^{I} V_{\text{f}}^{I} E_{\text{f}}^{I} \tag{15}$$

where η_{θ}^{I} and η_{l}^{I} are orientation and finite length efficiency factors for fibre system I, respectively. The influence from the fibre reinforcement on Poisson's ratio is assumed to be negligible.

According to [5] the tensile strength of the FRC material is assumed to be a function of the structural crack density parameter β_1 and two empirical calibration factors μ and σ_{β}. The factor μ makes it possible to take into account stress concentrations at the rebar/FRC interface due to the ribbed surface of the rebar, while the factor σ_{β} takes into account the hardening effect during progressive cracking and can be considered a measure of the statistical variation of the tensile strength in the FRC material in the axial direction of the prism.

Accordingly:

$$\sigma^{u}_{frc} = \mu\sigma_c(0) + \beta_1\sigma_\beta \quad (16)$$

and

$$\sigma^{crk}_{frc}(w) = \mu\sigma_c(w) \quad (17)$$

Throughout the present study the following parameter values have been used: $\eta_\theta = 1/5$ and $\eta_1 = 1.0$ corresponding to 3D randomized, fairly long fibres. For Poisson's ratio ν_{frc} the standard value of 0.2 has been used. According to [5] we have used $\mu = 0.5$ and $\sigma_\beta = 1$ MPa.

4. MATERIAL AND STRUCTURAL OPTIMIZATION

The starting point for material and structural optimization is typically determination of the micromechanical bond parameters by comparison with experimental results for the stress–crack width relationship. In order to demonstrate the capability of the proposed model for the stress–crack width relationship a comparison is made with experimental results reported in [5] for high strength concrete (called matrix III, see Table 1 for a description of the composition) with 1 and 3 vol. % of 12.5 mm long steel fibres with a diameter of 0.4 mm. The bond parameters (friction–slip relationship), the snubbing coefficient and the Cook–Gordon parameter were fixed in accordance with previous experience, see [6], and all the parameters are summarized in Table 2. The micromechanical parameters describing the fibre properties and the matrix (plain concrete) properties are summarized in Tables 3 and 1. These parameters, on the other hand, are all determined independently through direct physical testing. Comparisons for the two different fibre volume concentrations are shown in Figs 2 and 3.

Note that very good agreement with experimental data for the stress–crack width relation is obtained using parameters very close to the previously used parameters describing a different set of experiments [6]. In fact, the only difference is the use of $\tau_0 = 6$ MPa in the present case as compared with $\tau_0 = 4.2$ MPa in [6]. This difference corresponds well to the difference in matrix composition since matrix III was specially developed to obtain high paste density and bond. The interfacial parameters for the polypropylene (PP) fibres are taken directly from [6].

When the micromechanical bond parameters have been fixed the effect of fibre geometry can be studied, as shown in Fig. 4 where the fibre length has been changed. It is clear from this figure that the stress level for a given crack width is lowered by reducing the fibre length to 6 mm, and raised by increasing the fibre length to 18 mm and 24 mm. However, when further increasing the fibre length the stress–crack width relation deteriorates for crack widths larger than 0.05 mm due to fibre rupture. In fact, for crack widths larger than 0.1 mm the 36 mm fibre is no more efficient than the 18 mm fibre. Furthermore, it is noted that with increasing fibre length a distinct bump around $w = 0.05$ mm is produced. The curves suggest that the optimum fibre length is larger than 12.5 mm and in the following investigations an 18 mm steel fibre is considered.

The possibility of changing fibre volume concentration and/or combining/exchanging steel fibres with polypropylene (PP) fibres is explored in Fig. 5, where

Table 1 Mix proportions and material parameters for matrix III [5]

Mix proportions	
Cement	320 kg m^{-3}
Silica	41.3 kg m^{-3}
Clay	16.8 kg m^{-3}
Sand	896 kg m^{-3}
Gravel	1014 kg m^{-3}
Superplasticizer	25 kg m^{-3}
Water	95 kg m^{-3}
Material properties	
E_m	45 GPa
σ_{mu}	4.8 MPa
w_0	0.015 mm
p	1.5

Table 2 Material parameters: interfacial data for high tenacity polypropylene (PP) fibres and straight steel fibres [6]

Fibre system	τ_0 (MPa)	a_1 (MPa mm^{-1})	a_2 (MPa mm^{-2})	f	α (mm)
PP fibres	0.8	0	0	0.05	0.72
Steel fibres	6	−4	1	0.75	6

Table 3 Material parameters: fibre data for high tenacity polypropylene (PP) fibres and straight steel fibres

Fibre system	E_f (GPa)	σ_{fu} (MPa)	V_f (%)	L_f (mm)	d_f (mm)
PP fibres	11.9	400	1, 2	12	0.048
Steel fibers	210	1350	1, 2, 3	6, 12.5, 18, 24, 30, 36	0.4

Parameters in theoretical prediction (fat line):

E_m = 45 GPa σ_{mu} = 4.8 MPa w_0 = 0.015 mm p = 1.5
E_f = 210 GPa σ_{fu} = 1350 MPa V_f = 1.0 % L_f = 12.5 mm d_f = 0.4 mm
τ_0 = 6.0 MPa a_1 = -4 MPa/mm a_2 = 1 MPa/mm² f = 0.75 α = 6 mm

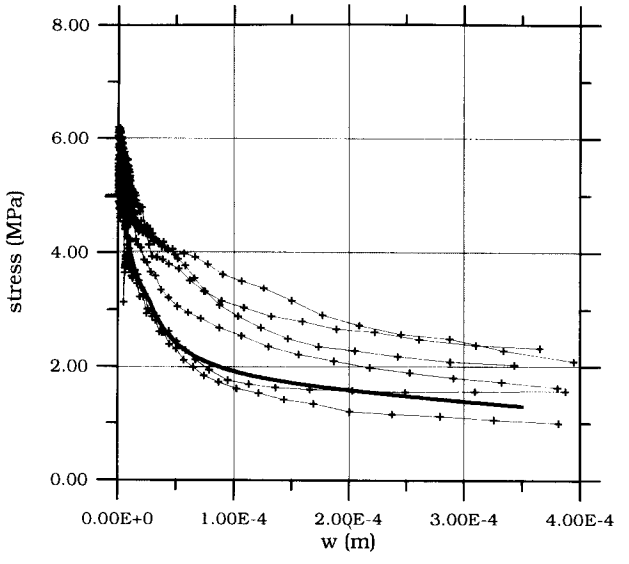

Fig. 2 Comparison between experimentally determined stress–crack width relationships (6 tests) for high strength concrete containing 1 vol. % of steel fibres (length 12.5 mm and diameter 0.4 mm; [5], matrix III at 28 days) and the theoretical prediction using the micromechanical parameters in Tables 3, 2 and 1.

Parameters in theoretical prediction (fat line):

E_m = 45 GPa σ_{mu} = 4.8 MPa w_0 = 0.015 mm p = 1.5
E_f = 210 GPa σ_{fu} = 1350 MPa V_f = 3.0 % L_f = 12.5 mm d_f = 0.4 mm
τ_0 = 6.0 MPa a_1 = -4 MPa/mm a_2 = 1 MPa/mm² f = 0.75 α = 6 mm

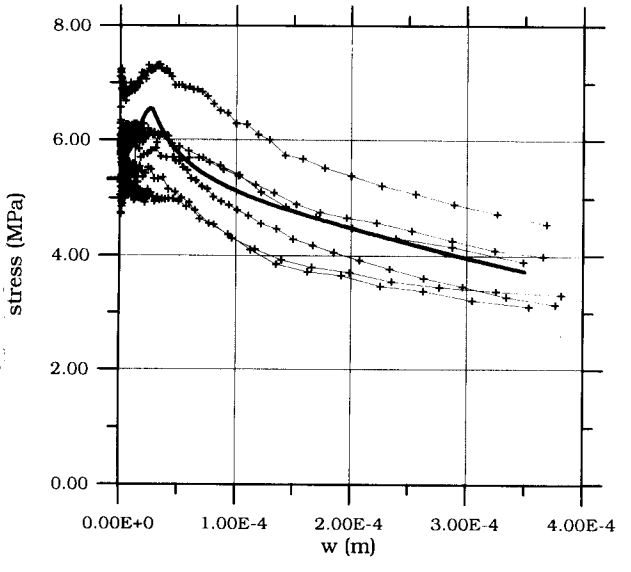

Fig. 3 Comparison between experimentally determined stress–crack width relationships for high strength concrete (6 tests) containing 3 vol. % of steel fibres (length 12.5 mm and diameter 0.4 mm; [5], matrix III at 28 days) and the theoretical prediction using the micromechanical parameters in Tables 3, 2 and 1.

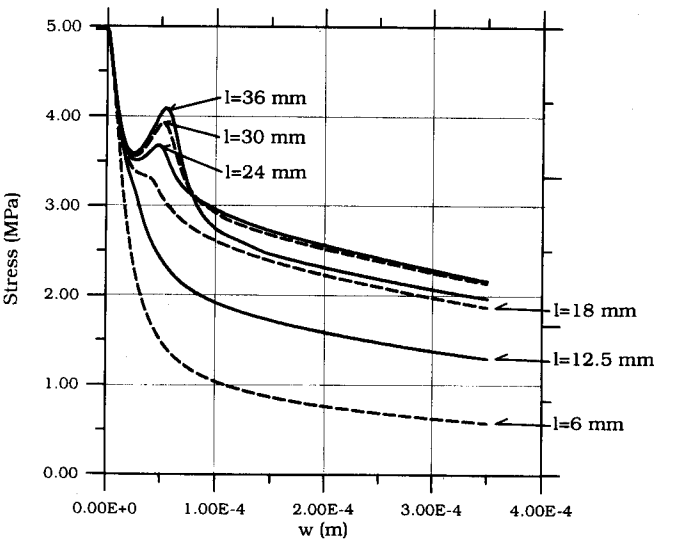

Fig. 4 Theoretically predicted stress–crack width curves for high strength concrete ([5], matrix III at 28 days) containing 1 vol. %, 0.4 mm diameter steel fibres using the micromechanical parameters in Tables 3, 2 and 1. Stress–crack width curves are shown for fibre lengths of 6 mm, 12.5 mm, 18 mm, 24 mm, 30 mm, and 36 mm.

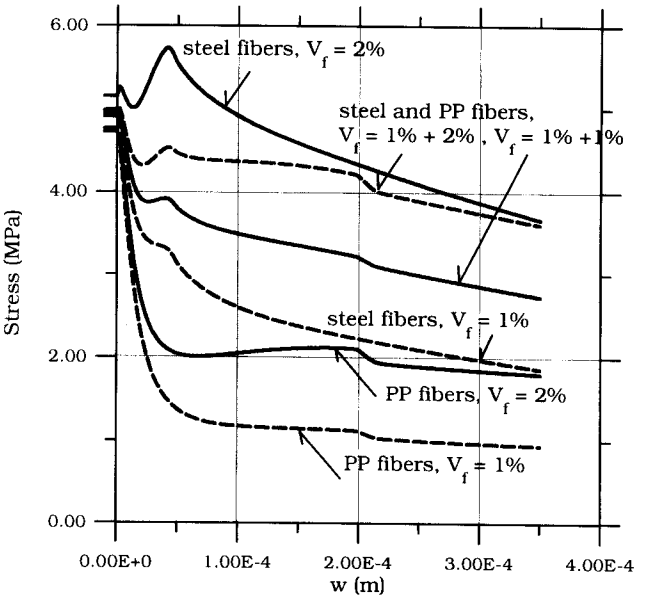

Fig. 5 Theoretically predicted stress–crack width curves for high strength concrete ([5], matrix III at 28 days) containing 18/0.4 mm steel fibres at volume concentrations of 1% and 2%, 12/0.048 mm polypropylene fibres at volume concentrations of 1% and 2%, and furthermore combinations of 1% of steel fibres and 1% and 2% of polypropylene fibres. The micromechanical parameters in Tables 3, 2 and 1 have been used throughout the study.

stress–crack width curves for 18 mm long steel fibres in volume concentrations of 1% and 2% are shown together with stress–crack width curves for the same amounts of PP fibres, 12 mm long and with 0.048 mm equivalent diameter. The properties of the PP fibres correspond directly to the polypropylene fibres investigated in [6], see Tables 3 and 2. Finally, the possibility of combining

1 vol. % of steel fibres with 1 vol. % and 2 vol. % of polypropylene fibres is investigated. It can be seen that, for crack widths larger than 0.2 mm, 2 vol. % of PP fibres roughly corresponds to 1 vol. % of steel fibres so that fibre concretes with 1 + 2% steel and PP fibres correspond to fibre concretes containing 2% of steel fibres. However, for crack widths around 0.05 mm the previously mentioned bump shows up in the curves for 2 vol.% steel fibres. The same pronounced bump is not observed in the 1 + 2% steel and PP fibre mix.

The stress–crack width curves can serve as guidelines for initial evaluation of the efficiency of different fibre systems. However, a true evaluation has to be made in connection with a specific structural application. In Figs 6 and 7 the structural crack widths as functions of stresses in the reinforcing bars are shown in a structure with an effective geometrical reinforcing degree $\phi = 0.03$, and a rebar diameter of 20 mm. The two figures show the structural crack widths in structures where the fibre reinforced concretes investigated in Figs 4 and 5 have been applied. Fig. 6 basically summarizes Fig. 4; with a fibre length of 6 mm (and 1 vol. %) no real change in structural crack widths can be expected compared with using plain concrete. However, if a fibre length of 18 mm is chosen some reduction in crack width (typically around 25%) will take place. It is confirmed furthermore that not much is gained by increasing fibre length over 18 mm.

As shown in Fig. 7, much more can be gained by increasing the fibre volume concentration. It is interesting to note that, even though 2 vol. % of PP fibres roughly correspond to 1 vol. % of steel fibres for crack widths larger than 0.2 mm, there is a big difference between using 2 vol. % of steel fibres and 1 + 2% of steel and PP fibres from a structural point of view. This is due to the relatively large difference in the curves around crack widths of 0.05 mm where the 2 vol. % of steel fibres shows a very pronounced bump to an extent that the stress levels exceed the initial tensile strength. This phenomenon reduces the crack widths drastically, and, as shown in Fig. 8, also reduces the distance between cracks to an extent where the crack pattern will probably be described as continuous microcracking rather than discrete macrocracking.

Assuming that the design criterion for a given structure is the mean crack width, the complete material structural optimization in terms of reinforcement can be done using diagrams as shown in Fig. 9, where crack width is shown as functions of both effective geometrical reinforcing degree of structural reinforcement and fibre reinforcement of the material for a given stress state (in this case 400 MPa) in the structural reinforcement. With a given crack width requirement, combinations of necessary structural and fibre reinforcement for different fibre systems can be determined directly or obtained from interpolation between the curves. Note in this connection that, using the fibre concrete with 2 vol. % of steel fibres, crack widths are virtually independent of the amount of structural reinforcement for the geometrical reinforcing degrees considered.

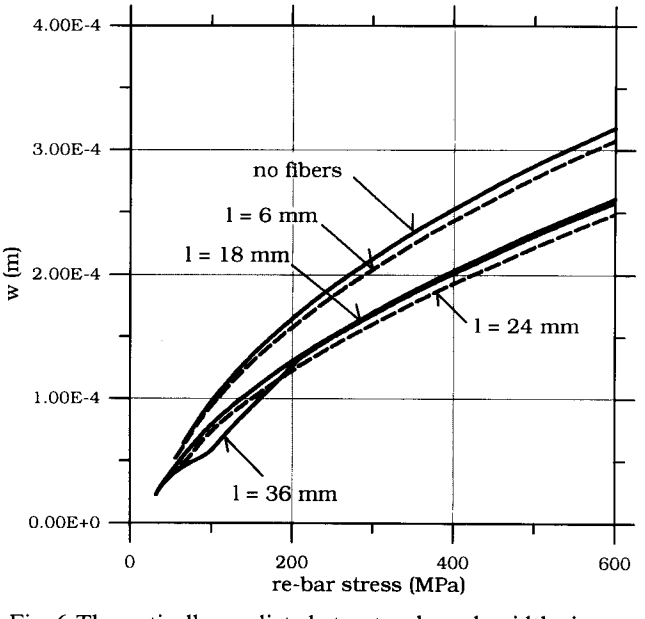

Fig. 6 Theoretically predicted structural crack widths in a structure with an effective geometrical reinforcing degree $\phi = 0.03$ and a rebar diameter ($2t$) of 20 mm. The crack widths are shown as functions of stress in the reinforcing bars for 4 of the fibre concretes shown in Fig. 4 (fibre lengths 6 mm, 18 mm, 24 mm, and 36 mm) along with the theoretical prediction for crack width in the concrete without fibres.

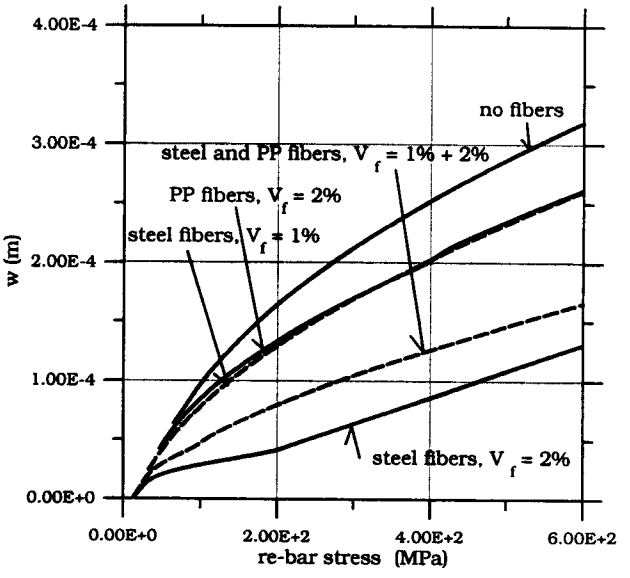

Fig. 7 Theoretically predicted structural crack widths in a structure with an effective geometrical reinforcing degree $\phi = 0.03$ and a rebar diameter ($2t$) of 20 mm. The crack widths are shown as functions of stress in the reinforcing bars for 4 of the fibre concretes shown in Fig. 5 (steel fibres $V_f = 1\%$ and 2%, polypropylene fibres $V_f = 2\%$, and a combination of steel and polypropylene fibres $V_f = 1\% + 2\%$) along with the theoretical prediction for crack width in the concrete without fibres.

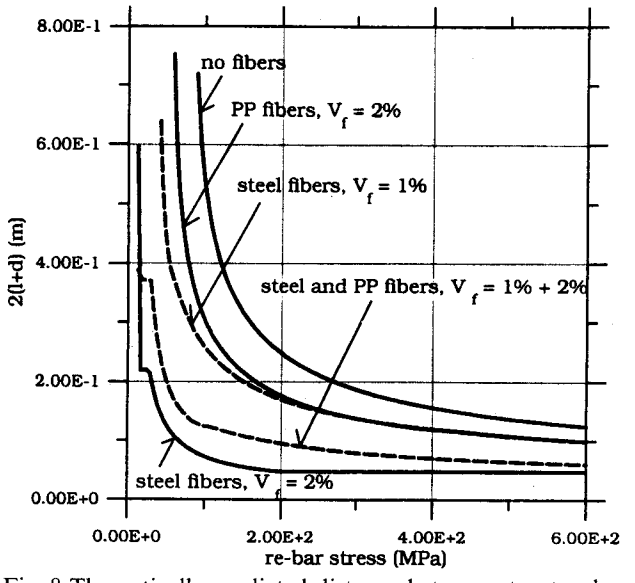

Fig. 8 Theoretically predicted distance between structural cracks in a structure with an effective reinforcing degree $\phi = 0.03$ and a rebar diameter ($2t$) of 20 mm. The crack distances are shown as functions of stress in the reinforcing bars for the same (fibre) concretes as shown in Fig. 7; steel fibres $V_f = 1\%$ and 2%, polypropylene fibres $V_f = 2\%$, and a combination of steel and polypropylene fibres $V_f = 1\% + 2\%$ along with the concrete without fibres.

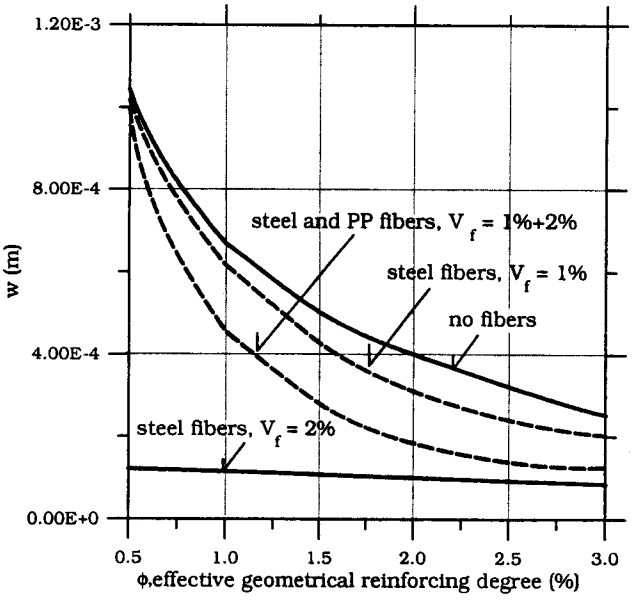

Fig. 9 The relation between structural crack widths and effective geometrical reinforcing degree ϕ for 4 of the concretes investigated in Fig. 7: steel fibres $V_f = 1\%$ and 2%, a combination of steel and polypropylene fibres $V_f = 1\% + 2\%$ along with the concrete without fibres. Rebar diameter is 20 mm and the design stress in the reinforcing bars is 400 MPa.

5. CONCLUSIONS

1. A model for the stress–crack width relationship for fibre reinforced concrete has been presented. The model is capable of taking fibre rupture and hybrid fibre systems into account, through a series of micromechanical parameters.
2. The stress–crack width relationship developed has been included in a model for structural crack widths, making it possible to predict cracks at the structural level taking not only geometrical design parameters as input but also parameters describing the material composition, i.e., choice of fibre system.
3. It is shown that a true evaluation of the efficiency of a given fibre reinforcement system can be evaluated only in a specific structural context. It is furthermore demonstrated that small differences in the stress–crack width relationship can have large effects in a given structural application.
4. A diagram has been constructed which can form the basis of material structural optimization with regard to choice of material and structural reinforcing system, provided that the design criterion is expressed in terms of mean (or possibly maximum) crack width.

ACKNOWLEDGEMENTS

H. S. and V. C. L. wish to thank NATO International Scientific Exchange Programmes, Collaborative Research, grant No. 930023, and the University of Michigan Rackham School of Graduate Studies Program to Promote International Partnerships for making the collaborative research possible. Part of the work on fibre rupture modelling has been carried out under a grant from the US National Science Foundation, grant No. BCS-9202097, to the University of Michigan. Helpful input by M. Maalej is gratefully acknowledged.

APPENDIX A: EXPRESSIONS FOR FIBRE BRIDGING STRESS

A.1 $2L_c e^{-f\pi/2} \le L_f \le 2L_c$

A.1.1 For $\hat{\delta} \le \hat{\delta}_c e^{-f\pi}$

$$\sigma_f = \sigma_0 g\left[2\left(\frac{\hat{\delta}}{\hat{\delta}^*}\right)^{1/2} - \left(\frac{\hat{\delta}}{\hat{\delta}^*}\right) + \hat{\delta}^2 - \tfrac{4}{3}\hat{\delta}^*\left(\frac{\hat{\delta}}{\hat{\delta}^*}\right)^{3/2} - \tfrac{2}{3}\hat{\delta}^*\hat{\delta}^3\right]$$

A.1.2 For $\hat{\delta}_c e^{-f\pi} \le \hat{\delta} \le \hat{\delta}^*$

$$\sigma_f = \sigma_0\left\{g(\Phi_c)\left[2\left(\frac{\hat{\delta}}{\hat{\delta}^*}\right)^{1/2} - \left(\frac{\hat{\delta}}{\hat{\delta}^*}\right) + \hat{\delta}^2 - \tfrac{4}{3}\hat{\delta}^*\left(\frac{\hat{\delta}}{\hat{\delta}^*}\right)^{3/2} - \tfrac{2}{3}\hat{\delta}^*\hat{\delta}^3\right] + \hat{L}_c^2 a(-f) - 2\hat{L}_c a(0)\hat{\delta} + a(f)(1 - \tfrac{2}{3}\hat{\delta}^*\hat{\delta})\hat{\delta}^2 + \tfrac{2}{3}\hat{L}_c^3 a(-2f)\hat{\delta}^*\right\}$$

A.1.3 For $\hat{\delta}^* \le \hat{\delta} \le \hat{L}_c e^{-f\pi/2}$

$$\sigma_f = \sigma_0\{g(\Phi_b)[(1 - \hat{\delta})^2 + \tfrac{2}{3}\hat{\delta}^*(1 - \hat{\delta}^3)] + \hat{L}_c^2 b(-f) - 2\hat{L}_c b(0)\hat{\delta} + b(f)(1 - \tfrac{2}{3}\hat{\delta}^*\hat{\delta})\hat{\delta}^2 + \tfrac{2}{3}\hat{L}_c^3 b(-2f)\hat{\delta}^*\}$$

A.1.4 For $\hat{L}_c e^{-f\pi/2} \le \hat{\delta} \le 1$

$$\sigma_f = \sigma_0\{g(\Phi_b)[(1-\hat{\delta})^2 + \tfrac{2}{3}\hat{\delta}^*(1-\hat{\delta}^3)] + \hat{L}_c^2 c(-f) - 2\hat{L}_c c(0)\hat{\delta} + c(f)(1-\tfrac{2}{3}\hat{\delta}^*\hat{\delta})\hat{\delta}^2 + \tfrac{2}{3}\hat{L}_c^3 c(-2f)\hat{\delta}^*\}$$

A.2 $L_f > 2L_c$

A.2.1 For $\hat{\delta} \le \hat{\delta}_c e^{-f\pi}$

$$\sigma_f = \sigma_0 g\left[2\left(\frac{\hat{\delta}}{\hat{\delta}^*}\right)^{1/2} - \left(\frac{\hat{\delta}}{\hat{\delta}^*}\right) + \hat{\delta}^2 - \tfrac{4}{3}\hat{\delta}^*\left(\frac{\hat{\delta}}{\hat{\delta}^*}\right)^{3/2} - \tfrac{2}{3}\hat{\delta}^*\hat{\delta}^3\right]$$

A.2.2 For $\hat{\delta}_c e^{-f\pi} \le \hat{\delta} \le \hat{\delta}_c$

$$\sigma_f = \sigma_0\left\{g(\Phi_c)\left[2\left(\frac{\hat{\delta}}{\hat{\delta}^*}\right)^{1/2} - \left(\frac{\hat{\delta}}{\hat{\delta}^*}\right) + \hat{\delta}^2 - \tfrac{4}{3}\hat{\delta}^*\left(\frac{\hat{\delta}}{\hat{\delta}^*}\right)^{3/2} - \tfrac{2}{3}\hat{\delta}^*\hat{\delta}^3\right] + \hat{L}_c^2 a(-f) - 2\hat{L}_c a(0)\hat{\delta} + a(f)(1-\tfrac{2}{3}\hat{\delta}^*\hat{\delta})\hat{\delta}^2 + \tfrac{2}{3}\hat{L}_c^3 a(-2f)\hat{\delta}^*\}$$

A.2.3 For $\hat{\delta}_c \le \hat{\delta} \le \hat{L}_c e^{-f\pi/2}$

$$\sigma_f = \sigma_0\{\hat{L}_c^2 g_1 - 2\hat{L}_c\hat{\delta} + g(1-\tfrac{2}{3}\hat{\delta}^*\hat{\delta})\hat{\delta}^2 + \tfrac{2}{3}\hat{L}_c^3 g_2\hat{\delta}^*\}$$

A.2.4 For $\hat{L}_c e^{-f\pi/2} \le \hat{\delta} \le \hat{L}_c$

$$\sigma_f = \sigma_0\{\hat{L}_c^2 d(-f) - 2\hat{L}_c d(0)\hat{\delta} + d(f)(1-\tfrac{2}{3}\hat{\delta}^*\hat{\delta})\hat{\delta}^2 + \tfrac{2}{3}\hat{L}_c^3 d(-2f)\hat{\delta}^*\}$$

Where

$$g = \frac{2}{4+f^2}[1+e^{f\pi/2}] \qquad g_1 = \frac{2}{4+f^2}[1+e^{-f\pi/2}]$$

$$g_2 = \frac{1}{2(1+f^2)}[1+e^{-f\pi}]$$

$$\Phi_c = -\frac{1}{2f}\log\left(\frac{\hat{\delta}}{\hat{\delta}_c}\right) \qquad \Phi_b = -\frac{1}{f}\log\left(\frac{L_f}{2L_c}\right)$$

$$\Phi_a = -\frac{1}{f}\log\left(\frac{\hat{\delta}}{\hat{L}_c}\right)$$

$$g(\Phi_c) = \frac{1}{4+f^2}\{[f\sin(2\Phi_c) - 2\cos(2\Phi_c)]e^{f\Phi_c} + 2\}$$

$$a(f) = \frac{1}{4+f^2}\{[2\cos(2\Phi_c) - f\sin(2\Phi_c)]e^{f\Phi_c} + 2e^{f\pi/2}\}$$

$$b(f) = \frac{1}{4+f^2}\{[2\cos(2\Phi_b) - f\sin(2\Phi_b)]e^{f\Phi_b} + 2e^{f\pi/2}\}$$

$$c(f) = \frac{1}{4+f^2}\{[f\sin(2\Phi_a) - 2\cos(2\Phi_a)]e^{f\Phi_a} + [2\cos(2\Phi_b) - f\sin(2\Phi_b)]e^{f\Phi_b}\}$$

$$d(f) = \frac{1}{4+f^2}\{[f\sin(2\Phi_a) - 2\cos(2\Phi_a)]e^{f\Phi_a} + 2\}$$

$$\hat{\delta}^* = \frac{2\tau L_f}{E_f d_f(1+\eta)} \qquad \hat{\delta}_c = \frac{\sigma_{fu}^2 d_f}{4E_f\tau(1+\eta)} = \hat{L}_c^2\hat{\delta}^*$$

$$\sigma_0 = \frac{V_f\tau L_f}{2d_f} \qquad \hat{\delta} = \frac{\delta}{L_f/2} \qquad L_c = \frac{\sigma_{fu}d_f}{4\tau}$$

$$\hat{L}_c = \frac{L_c}{L_f/2} \qquad \eta = \frac{V_f E_f}{V_m E_m} \qquad G_0 = \frac{V_f\tau L_c^2}{d_f}$$

APPENDIX B: LIST OF SYMBOLS

a_1	First coefficient in polynomial expression for interfacial friction
a_2	Second coefficient in polynomial expression for interfacial friction
b	Thickness of concrete in structural crack width model
d	Half length of rebar–concrete debonded zone
d_f	Fibre diameter
E_f	Young's modulus of the fibres
E_{frc}	Young's modulus for fibre concrete
E_m	Young's modulus of the matrix
E_s	Young's modulus of structural reinforcing bars
f	Snubbing coefficient
l	Half crack spacing without rebar–concrete debonding
L_f	Fibre length
N	Number of cracks in structural crack width model
p	Shape factor in empirical stress–crack width relationship
t	Radius of structural reinforcing bar
V_f	Fibre volume concentration
w	Crack width
w_0	Characteristic crack width in empirical stress–crack width relationship
α	Cook–Gordon parameter (length of fibre–matrix debonded zone)
β_1	Structural crack density parameter
δ	Crack opening in model without Cook–Gordon effect
δ^*	Crack opening corresponding to complete debonding of all fibres
ε_{mu}	First crack strain of plain concrete
η_1	Finite length efficiency factor in composite material stiffness calculation
η_θ	Orientation efficiency factor in composite material stiffness calculation
μ	Empirical calibration factor in structural stress–crack width model
ν_{frc}	Poisson's ratio for fibre concrete
ν_s	Poisson's ratio for structural reinforcing bars
σ_a	Stress carried across a crack due to aggregate bridging
σ_c	Stress carried across a crack in the micromechanical model
σ_f	Stress carried across a crack due to fibre bridging
σ_{frc}^{crk}	Stress transferred across a crack in the structural calculation
σ_{frc}^{u}	First crack strength of fibre concrete
σ_{fu}	Tensile strength of the fibres
σ_{mu}	First crack strength of plain concrete

σ_{ps} Stress carried across a crack due to fibre pre-stress
σ_{ps}^{0} Fibre pre-stress before debonding
σ_{β} Empirical calibration factor in structural first crack strength model
τ Interfacial frictional resistance
τ_0 Constant in polynomial expression for interfacial friction
ϕ Structural geometrical reinforcing degree

REFERENCES

1. Romualdi, J. P. and Batson, G. B., 'Mechanics of crack arrest in concrete', *ASCE J. Engng Mech. Div.* **89** (1963) 147–168.
2. Bentur, A. and Mindess, S., 'Fiber Reinforced Cementitious Composites' (Elsevier Applied Science, Barking, UK, 1990) p. 449.
3. Balaguru, P. N. and Shah, S. P., 'Fiber Reinforced Cement Composites' (McGraw-Hill, New York, 1992) p. 530.
4. Stang, H., 'Evaluation of properties of cementitious fiber composite materials', in 'High Performance Fiber Reinforced Cement Composites', edited by H. W. Reinhardt and A. E. Naaman (E & FN Spon, London, 1992) pp. 388–406.
5. Stang, H. and Aarre, T., 'Evaluation of crack width in FRC with conventional reinforcement', *Cement Concr. Comp.* **14** (1992) 143–154.
6. Li, V. C., Stang, H. and Krenchel, H., 'Micromechanics of crack bridging in fibre reinforced concrete, *Mater. Struct.* **26** (1993) 486–494.
7. Hillerborg, A., Modéer, M. and Petersson, P. E., 'Analysis of crack formation and crack growth in concrete by means of fracture mechanics and finite elements', *Cement Concr. Res.* **6** (1976) 773–782.
8. Hillerborg, A., 'Analysis of fracture by means of the fictitious crack model, particularly for fibre reinforced concrete', *Int. J. Cement Comp.* **2** (1980) 177–184.
9. Li, V. and Liang, E., 'Fracture processes in concrete and fibre reinforced cementitious composites', *ASCE J. Engng Mech.* **122** (1986) 566–586.
10. Li, V. C., Post-crack scaling relations for fibre reinforced cementitious composites', *ASCE J. Mater. Civil Engng* **4** (1992) 41–57.
11. Cook, J. and Gordon, J. E., 'A mechanism for the control of crack propagation in all brittle systems', *Proc. R. Soc. Lond.*, **282A**, (1964) 508–520.
12. Maalej, M., Li, V. C. and Hashida, T., 'Effect of fiber rupture on tensile properties of short fiber composites, unpublished.
13. 'Code of Practice for the Structural Use of Concrete, DS 411' (Teknisk Forlag, Copenhagen, 1984).
14. Krenchel, H., 'Fibre Reinforcement' (Akademisk Forlag, Copenhagen, 1964) p. 159.

RESUME

Calcul et applications structurelles des relations contrainte–largeur des fissures dans le béton armé de fibres

La relation contrainte–largeur de fissure est essentielle pour la compréhension de la progression de la fissuration et du comportement mécanique en traction des matériaux et des structures en béton renforcé de fibres. On propose un modèle de la relation contrainte–largeur de fissure de composites à fibres courtes avec une orientation aléatoire. Ce modèle prend en compte des compositions hybrides et des ruptures possibles des fibres. On démontre comment cette relation contrainte–largeur de fissure peut être incluse dans un modèle structural de prédiction de la largeur des fissures dans une structure en béton armé. Avec cette combinaison de modèles, on a créé un instrument rationnel pour le calcul des matériaux et des structures composites. On démontre comment des systèmes différents de fibre peuvent être analysés par rapport à leur applicabilité structurale, et comment il est possible d'effectuer une optimalisation combinée du côté matériaux et du côté structures.